FOREX Publication
Open Access | Rapid and quality publishing

International Journal of
Electrical and Electronics Research (IJEER)
Research Article | Volume 11, Issue 4 | Pages 979-987 | e-ISSN: 2347-470X

Design and Implementation of a Two-Frequency Power Amplifier without Interference for Wireless Communication

Wael Saad Ahmed[1], Nsaif Jasim Hadi Al-Chaabawi[2], and Ahmed Atiyah Itwayya[3]

[1]*University of Tikrit, Salahaddin, Iraq*
[2]*College of Engineering, Department of Petroleum, University of Misan, Amarah, Iraq*
[3]*Ministry of Electricity General Company for Southern Electricity Distribution – Maysan Branch*

***Correspondence:** wael.alrawi@tu.edu.iq;

ABSTRACT- In this research paper, we will delve into a type of circuit known as a power amplifier. This circuit is designed to operate at two frequencies, allowing it to perform tasks at each frequency. The main goals of the design are to separate signals and ensure proper operation of the circuit in different modes. One notable feature of this power amplifier is its ability to work without any distortion, especially when both frequencies are used simultaneously. Achieving this has been made possible by combining a method that ensures signal termination with a strategy that enables their separation. To evaluate its performance, we conducted computer simulations as tests using both large signals. The findings indicate a 10.2 decibel increase in amplification, with an output power of 41.2 decibels measured in milliwatts (dBm) and an overall power efficiency of 40.2% at a frequency of 1.8 gigahertz. Furthermore, our research reveals that the suppression of signals for the 1.8 GHz band is reduced by 49 decibels compared to the original signal, while for the 2.6 GHz band, almost all traces of the second harmonic signal are completely eliminated. In addition, we propose a circuit that mitigates mixing outcomes and enhances linearity performance. The EDA software, Path Wave EM Design, is used for simulation purposes.

Keywords: Dual -Frequency Operation; Signal Division; Distortion-Free; Power Efficiency; Power Amplifier; Wireless Communication.

ARTICLE INFORMATION

Author(s): Wael Saad Ahmed, Nsaif Jasim Hadi Al-Chaabawi and Ahmed Atiyah Itwayya;

Received: 16/09/23; **Accepted**: 16/10/23; **Published**: 07/11/23;
E- ISSN: 2347-470X;
Paper Id: IJEER230733;
Citation: 10.37391/IJEER.110415
Webpage-link:
https://ijeer.forexjournal.co.in/archive/volume-11/ijeer-110415.html

Publisher's Note: FOREX Publication stays neutral with regard to jurisdictional claims in Published maps and institutional affiliations.

1. INTRODUCTION

Creating mobile communication systems can pose challenges due to the need to address hardware issues. One crucial aspect of these systems is to ensure that power amplifiers can function effectively across bands. However, when multiple bands are used simultaneously, the power amplifier may encounter modulation problems, resulting in distorted output signals. This issue significantly impacts the accuracy of power amplifiers in communication systems. Therefore, developing a power amplifier that can operate reliably and deliver optimal performance across various frequency ranges is a challenging task [1–2]. To tackle these challenges, innovative techniques such as Doherty, Envelope Tracking, and Out phasing have been developed [3-4].

The development of the Doherty Power Amplifier (DPA) aims to enhance both accuracy and performance. Notably the DPA offers an advantage by maintaining precision, under high power conditions [5]. However due to its manufacturing process it is unsuitable for applications like FM, FSK and PSK. Additionally, the DPA has limited capacity for data transmission. In terms of power amplifiers, Envelope Tracking leverages the development of the Doherty Power Amplifier (DPA) to enhance both accuracy and performance. Notably, the DPA offers an advantage by maintaining precision under high-power conditions [5]. However, due to its manufacturing process, it is unsuitable for applications such as FM, FSK, and PSK. Additionally, the DPA has a limited capacity for data transmission. In terms of power amplification, Envelope Tracking power amplifiers effectively leverage the output power of RF power amplifiers [6]. By regulating the power, they receive, ET amplifiers ensure that they operate close to their maximum power capacity. This approach provides benefits such as compatibility with various frequencies and high efficiency [7]. However, there are disadvantages connected with ET amplifiers. This implies that certain components within a system may encounter difficulties in functioning due to variations in their power levels. The phasing power amplifier consists of two amplifiers that amplify signals in different ways to increase their size [8]. This technique allows for the restoration of the input signal envelope, with increased amplitude and overall efficiency. Since the signal envelope loses information after being divided, it becomes possible to utilize high-efficiency power amplifiers to achieve a balance between efficiency and linearity [9].

However, developing power combiners that offer optimal performance and yield satisfactory outcomes can prove to be

FOREX Publication
Open Access | Rapid and quality publishing
International Journal of Electrical and Electronics Research (IJEER)
Research Article | Volume 11, Issue 4 | Pages 979-987 | e-ISSN: 2347-470X

quite challenging, thereby impeding progress. Various alternative approaches have been suggested to enable power amplifiers to operate across different frequency bands. These research endeavors delve into the exploration of a technique known as end-to-end, which aims to eliminate second harmonics and enhance performance in both frequency ranges [10]. Nevertheless, these investigations have not yet addressed the issue of linearity, including the occurrence of cross modulation during dual-band operations. To achieve efficiency and linearity, it is imperative to use high-efficiency power amplifiers. This is because the signal envelope loses all relevant information when it is separated [11]. In this manuscript, we present a technological advancement that enhances the precision and effectiveness of dual-band amplifiers. Primarily, we employ an approach that optimizes the functioning of the device within two distinct frequency ranges. This strategic approach facilitates the elimination of any potential mixing effects that may arise during the device's operation [12]. By incorporating components, we are able to reduce harmonics and improve the overall functionality of the system. The circuit configuration is shown in *figure 1*. To achieve this objective, it is necessary to use a diplexer, which functions as a fundamental component. The diplexer effectively separates signals into two distinct frequencies, namely f1 and f2. Each individual signal is subsequently amplified separately using f1 and f2 amplifiers.

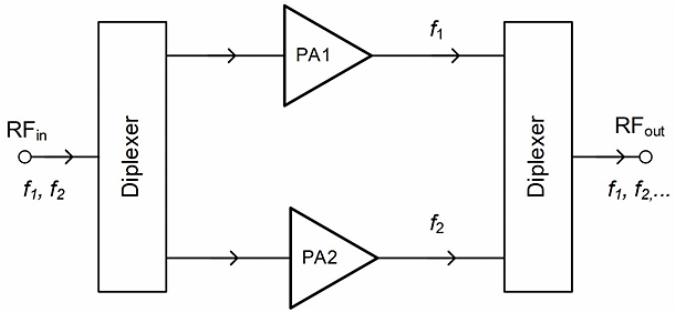

Figure 1: The picture of the dual-band power amplifier shows special components called diplexers at the beginning and end.

The purpose of using a diplexer is to eliminate distortion caused by intermodulation and cross modulation. In each amplifier, the output matching network is equipped with a circuit that reduces harmonics of the order. This ensures that the resulting frequencies of the power amplifier consist only of the frequency components. Through the use of a diplexer, we can separate signals and prevent two frequencies from entering the same active element, thereby eliminating intermodulation distortion effectively. Moreover, compared to wideband impedance circuits, the design of impedance harmonic suppression circuits in each branching power amplifier becomes simpler. This study applies this method to a power amplifier manufactured on a low-cost single-layer FR-4 substrate.

2. LITERATURE REVIEW

In order to demonstrate the feasibility of programmable meta surfaces in the design of future communication systems and to establish innovative wireless communication systems based on meta surfaces, several critical issues need to be addressed [13]. One of the main points relates to the introduction of a Line of Sight (LoS) communication pathway that connects unmanned aerial vehicles (UAVs) with the terrestrial network. This development has the potential to significantly disrupt the connection between the aerial and terrestrial domains. Furthermore, there are distinct requirements for the quality of service (QoS) of UAV control messages compared to payload data. In addition, the size, weight, and power (SWAP) limitations of UAVs impose strict constraints on the system design. Moreover, the highly controllable 3D mobility of UAVs opens up new design possibilities and degrees of freedom (DoF) that can be exploited. This tutorial provides an overview of recent advancements in UAV communications, with a focus on addressing the aforementioned issues. It highlights the integration of UAVs into the upcoming fifth-generation (5G) and future cellular networks [14]. Various transceiver configurations are analyzed by categorizing them into power-limited (PL) and power-spectral (PS) configurations [15]. The investigation of channel loss mitigation will involve developing a transmitter scheme that effectively utilizes the benefits of diversity technology by leveraging the statistical attributes of the transmitter's channel [16]. Several synchronization algorithms have been examined and deployed using a software-defined radio (SDR) that utilizes the Universal Software Radio Peripheral (USRP). The evaluation is based on the correlation of the symbols in the preamble [17]. In recent times, scholars have conducted investigations into various approaches aimed at improving the utilization of LDACS spectrum through filtering and windowing technology. In this context, a novel low-complexity LDACS system is proposed, based on the LRef-OFDM (Low-Complexity Reference OFDM) filter. The system employs multi-tier digital filters that rely on interpolation and masking techniques [18]. The hybrid design algorithm exhibits adaptability towards millimeter waves (mmwaves) and terahertz (THz) multi-user multiple-input multiple-output (MIMO) systems. This algorithm consists of separate computational stages for digital precoders, analog precoders, and multi-user interference mitigation [19].

A novel approach for dual-domain waveform design is proposed, which combines the legacy orthogonal frequency division multiplexing (OFDM) modulation scheme with a sensing signal specifically designed in the Delay-Doppler (DD) domain [20-21]. We hereby introduce a simplified and innovative blueprint for a temperature sensor that utilizes fiber optics, relying on the response exhibited by the localized surface plasmon resonance (LSPR). These sensors utilize cost-effective circuits, which consist of photodiodes, transimpedance amplifiers (TIAs), and overlapping light-emitting diodes (LEDs). This design holds particular promise for monitoring applications that prioritize minimizing deployment expenses [22-23]. We propose to develop cutting-edge lighting control systems that possess intelligent energy-saving capabilities, leveraging ZigBee and NB-IoT technology as their foundation [24-25].

FOREX Publication
Open Access | Rapid and quality publishing
International Journal of Electrical and Electronics Research (IJEER)
Research Article | Volume 11, Issue 4 | Pages 979-987 | e-ISSN: 2347-470X

3. METHODS PROCEDURAL GUIDELINES FOR DESIGNING

3.1 Circuits Diplexer

The circuits for diplexers and the power amplifiers themselves are produced on a substrate, which is commonly used for its cost-effectiveness. This specific substrate has a loss tangent value of 0.014 and a permittivity value of 4.5. The visual representation presented in *figure 2* illustrates the two constituent arms that form the diplexer. The left arm blocks signals at a frequency called *f1*, while allowing signals at another frequency referred to as *f2* to pass through. On the other hand, the right arm blocks signals at *f2*. Only signals at *f1* are allowed to pass through. The substrate has a thickness of 0.8 millimeters, while the other one measures 35 micrometers in thickness. The symbol λ represents the wavelength of a wave, measured in meters.

The Greek letter lambda is commonly used to represent the distance between two consecutive points on a wave. The velocity, v, at which the wave group propagates within the medium can be determined using *equation (1)*.

$$f(\lambda)=v/f \quad (1)$$

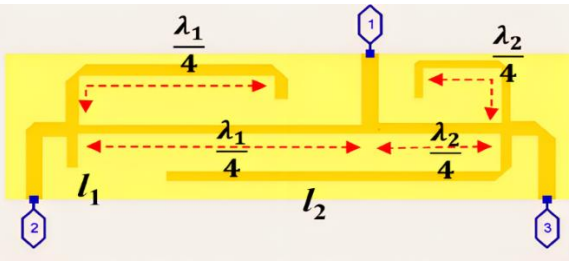

Figure 2: A diagram illustrating the diplexer is presented.

Each arm possesses two lines that are approximately one quarter of the wavelength in length in order to achieve this objective. This arrangement ensures that the *f1* and *f2* signals do not complete a circuit. Additionally, in order to reduce the impedance of the *f1* and *f2* signals, we have included two tubes, designated as *l1* and *l2*, in the design. The dimensions of the transmission line segments are precisely measured to be a quarter-wavelength, with a width of 1.47mm and a length of 21.6mm. On the adjacent side, the width of the quarter-wavelength tube is 1.14 mm, and the length is 19.3 mm. Moreover, the small section labeled *L1* measures 0.5 mm in width and 2.65 mm in length. The series arm features a secondary line that is 1.47 mm wide and 10.66 mm long, representing one quarter of the wavelength. Furthermore, it has a width of 0.88 mm and a length of 7.79 mm, measuring half-length. Lastly, the final tube, known as L2, has dimensions of 0.5 millimeters in width and 30.56 millimeters in length.

In *figure 3* we can see the design of the diplexer, on the base. In Port 1, two distinct frequencies, namely 1.8 gigahertz and 2.6 gigahertz, are incorporated. Discover the provided modules. These modules convert connections from Port 1 to connections from Ports 2 and 3, and they function as 50-ohm lines. The transformation takes place at frequencies denoted as *f2* and *f1*, respectively. This process is achieved by using stubs. They are a quarter of the wavelength in length and their reactance is adjusted. By adjusting the dimensions and sizes of these stubs, we can regulate the transmission of specific frequencies while blocking others.

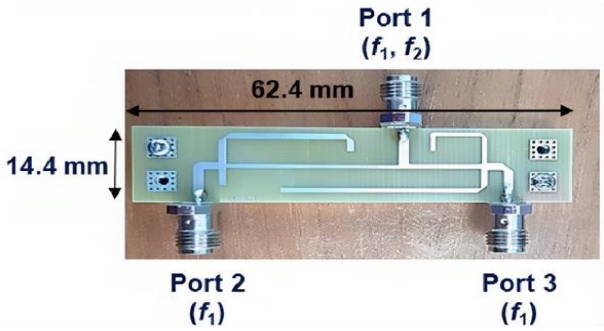

Figure 3: A constructed model of the diplexer on a budget-friendly FR-4 base material

The results of the diplexer design determined through both simulations and measurements are shown in *figure 4*.

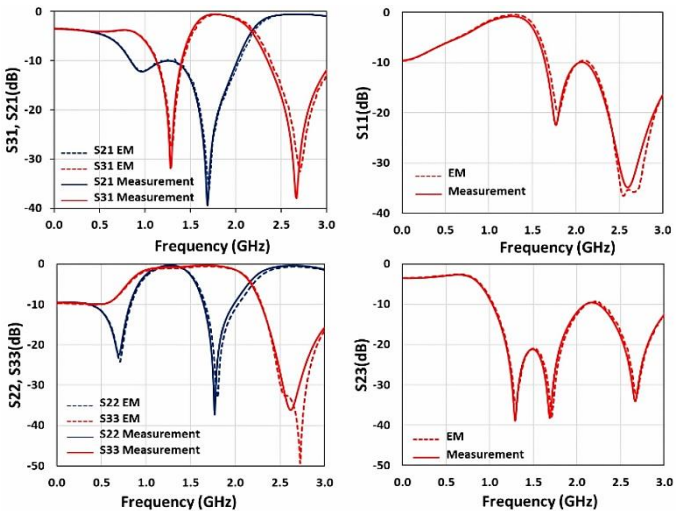

Figure 4: Simulation (EM) results and measurements of the diplexer S-parameters. The figure consists of four charts that display different measurements.

It has been demonstrated that the diplexer has been designed meticulously and is performing well as confirmed by both simulations and measurements. The slight variations observed between simulations and measurements can be explained by several factors, including joint and solder loss as well as FR 4 material degradation. However, upon examining the circuit, it becomes clear that it "conforms to expectations and is acceptable". The signal, at a frequency of 1.8 gigahertz has a loss in transmission 0.6 decibels. However, the loss is much higher at 2.6 GHz, measuring around 21.8 dB. Specifically, within the 2.6 GHz range, the transmitted signal experiences a decrease of 0.6 dB in comparison to its original strength. When the frequency reaches 18 gigahertz, there is an obstruction that causes a loss of approximately 21.4 dB in the

FOREX Publication
Open Access | Rapid and quality publishing
International Journal of Electrical and Electronics Research (IJEER)
Research Article | Volume 11, Issue 4 | Pages 979-987 | e-ISSN: 2347-470X

signal strength. The return losses at each port are considered acceptable since they are below 20 dB. Moreover, there is isolation between the output ports, as indicated by measurements exceeding 20 dB.

The charts are designed to facilitate the comparison of frequency values, which are labeled as "frequency (GHz)" to indicate that the measurements are in gigahertz. The charts are color-coded, with the red and blue lines representing frequency values. The charts are arranged side by side, making it easy to compare measurements and observe trends and patterns.

3.2 Solitary amplifier

The power amplifier employed in this specific design utilizes a sophisticated class-AB configuration. The electrical potential at the drain is referred to as the drain bias voltage, which has been set at 28 volts. Meanwhile, the gate bias voltage has been set to 1.94 volts. It is worth noting that impedance matching circuits are essential components of any power amplifier. To eliminate the second harmonic, open stubs are used to create purely reactive harmonic impedances, effectively blocking the second harmonic from reaching the device. In addition, the load/source attraction method is employed to determine the most optimal impedances for the input and output matching circuits. The diagram presented in *figure 5* depicts the schematic representation of a solitary amplifier. In this configuration, the *LS1* port serves the purpose of attenuating the second harmonic, while the *LS2* port aligns the 50 Ω impedance with the most optimal source impedance at the primary frequency.

We can calculate the value of ls using a mathematical formula *equation (2)*.

In a similar *L1 lL1 L2 lL2* on the output side serve same identical purpose as the stubs on the input side.

Figures 6 and 7, shown in the aforementioned figures, illustrate a pair of customized power amplifiers operating at frequencies of 1.8 and 2 GHz, respectively. The visual representations mentioned above demonstrate the close relationship between the input and output impedance, which is obtained from simulation, and the impedance obtained through circuitry. In *table 1*, the data pertaining to the measurements of stubs at frequencies of 1.8 GHz and 2.6 GHz is presented.

$$lS=\lambda/4 \qquad (2)$$

Table 1. Displays the dimensions of each individual amplifier, measured in millimeters.

Amplifier	1.8 GHz power amplifier	2.6 GHz power amplifier
W / l_{S1}	1.48/11.40	2/11.65
W / l_{S2}	1.48/12.9	2.1/9.54
W / l_{L1}	1.6/18.4	2.3/12
W / l_{L2}	1.9/14.8	2.6/10.1

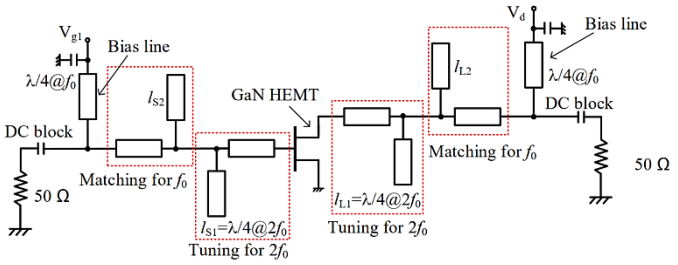

Figure 5: Shows a single amplifier with input and output matching networks, which have the remarkable ability to effortlessly handle harmonious second-order frequencies.

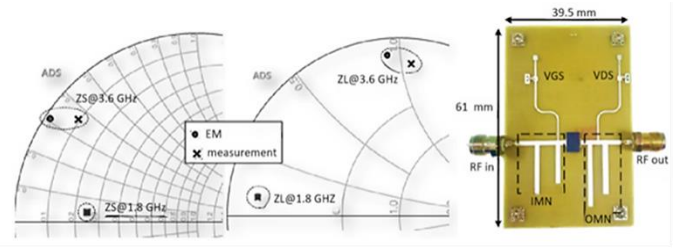

Figure 6: The real and simulated impedances are for a power amplifier operating at a frequency of 1.8 GHz.

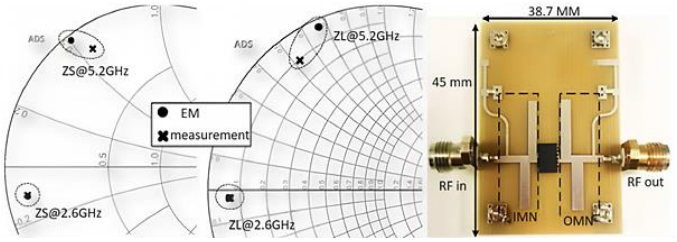

Figure 7: Impedances were simulated, measured, and subsequently an operational 2.6-GHz power amplifier was fabricated.

In *figure 8*, we can see how power amplifiers behave at different frequencies. These behaviors include power-added efficiency gain and output power (Pout). At a frequency of 1.77 GHz, the measured output power is 42.1 dBm, with a gain of 10.1 dB. Additionally, the maximum power-added efficiency (PAE) for a power amplifier operating at 1.8 GHz is determined to be 49%. Similarly, at a frequency of 2.59 GHz, we observe an efficiency of 44.5%, a gain of 10.7 dB, and an output power of 41.7 dBm for the power amplifier in question. The power amplifier is measured using the same parameters at a frequency of 2.6 GHz.

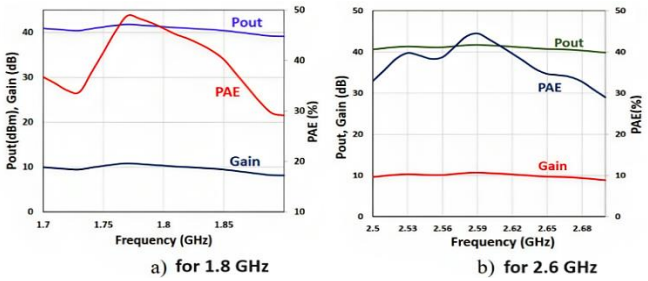

Figure 8: Features of the Frequency Response for Large Signals.

FOREX Publication
Open Access | Rapid and quality publishing
International Journal of Electrical and Electronics Research (IJEER)
Research Article | Volume 11, Issue 4 | Pages 979-987 | e-ISSN: 2347-470X

The integration of input/output filters with pre-existing individual power amplifiers led to the development of the dual-band power amplifier. A diagram of the first version of a power amplifier, which can operate on two different frequency ranges, is shown in *figure 9*. It has been made by someone. The circuit is small, measuring approximately 5.48 centimeters by 10.44 centimeters. *Figure 10* illustrates the procedure we used to conduct an experiment and obtain measurements of small signals. We use a machine called the Keysight Vector Network Analyzer N5242A to measure the performance of something at low levels. The measurements' findings are displayed in *figure 11*. It is important to mention that the results of electromagnetic simulations and measurements at the designated frequency bands are very similar. The gain at 1.8 GHz is 10.7 dB, and at 2.6 GHz it is 9.5 dB. The measurements of the big signal are performed using the equipment shown in *figures 12 and 13*.

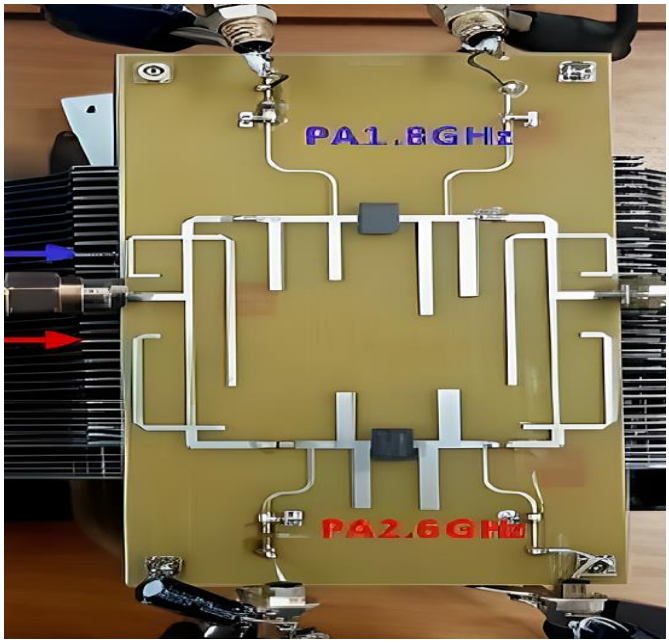

Figure 9: The dual-frequency power amplifier consists of a unique device called a diplexer, along with two separate amplifiers that operate independently

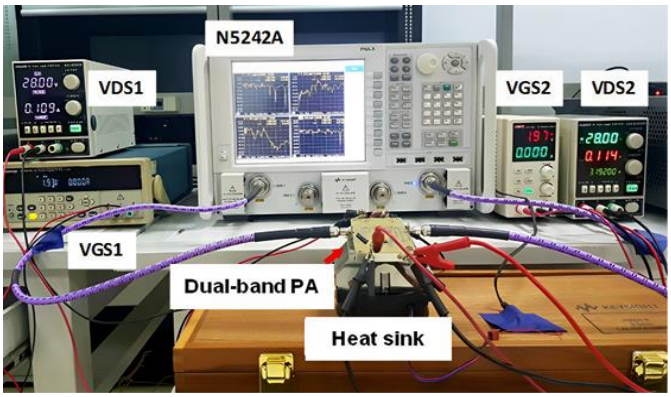

Figure 10: The diagram provides a visual representation of the configuration used to perform small signal analysis autonomously using the Keysight Vector Network Analyzer (N5242A).

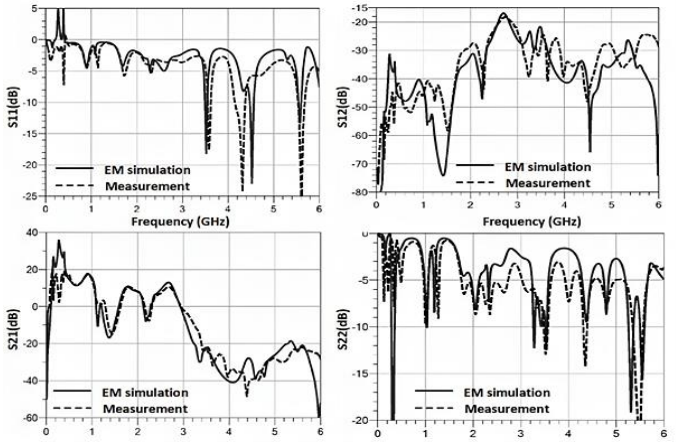

Figure 11: The small signal electrical test results of the dual band power amplifiers are showcased.

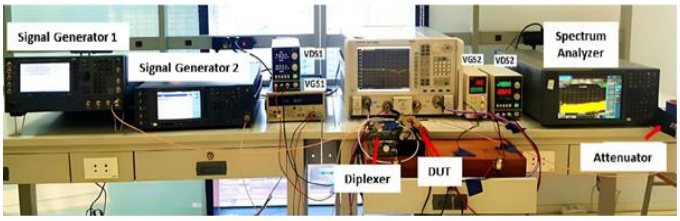

Figure 12: The diagram illustrates the setup used to evaluate the effectiveness of a newly developed dual-frequency power amplification device.

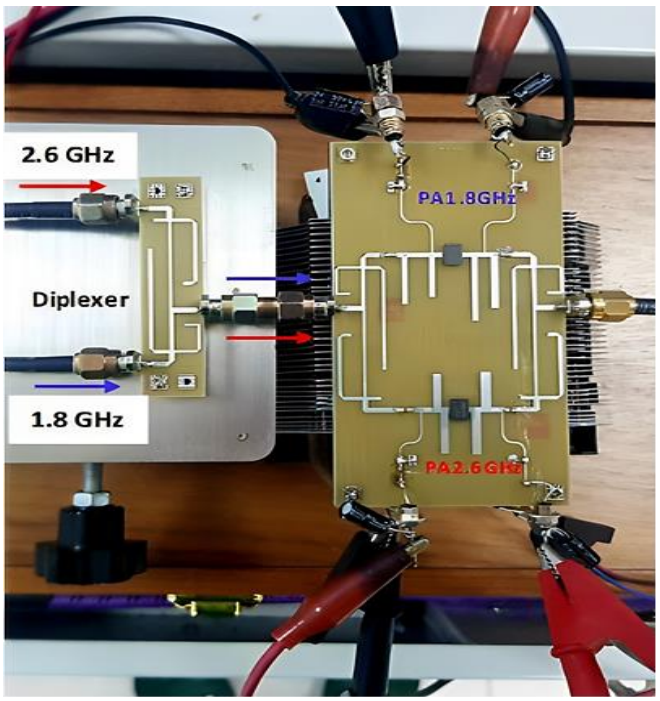

Figure 13: The power amplifier section that operates on two separate input signals, each with distinct frequencies of 1.8 GHz and 2.6 GHz, integrates them using a filter.

The input diplexer is connected to two signal generators in this specific configuration to transmit RF dual-band signals to the power amplifier. Subsequently, after the power amplifier

FOREX Publication
Open Access | Rapid and quality publishing
International Journal of Electrical and Electronics Research (IJEER)
Research Article | Volume 11, Issue 4 | Pages 979-987 | e-ISSN: 2347-470X

output is terminated, a spectrum analyzer is used to observe the resulting spectrum. The measurement technique is subject to limitations imposed by the RF signal transmitter operating within the laboratory, which has a maximum input limit of 20 dBm. Consequently, only the range of Pin from 10 dBm to 20 dBm is used to calculate the parameters required for large-signal measurement.

Figure 14 illustrates the significant characteristics of the power amplifier in terms of its power-added efficiency (PAE), output power (Pout), gain, and drain current (IDS). Although the presentation of the measured results is not comprehensive, they show a favorable alignment with the simulation. The use of FR-4 material results in a decrease in Pout when operating at high frequencies, thereby reducing both the gain and PAE at higher frequencies.

We thoroughly examined the performance of a power amplifier in a linear manner to assess the effectiveness of our proposed methodology. Our investigation primarily focused on the power amplifier's ability to reject mixing products and harmonic signals. The evidence indicates that the dual-band power amplifier provides a wider range of outputs compared to a single-band power amplifier, as shown in Figure 15. This increased range can be attributed to the use of a technique that splits signals and includes termination circuits in the dual-band power amplifier.

The results of this study are compared to the experiment depicted in *figure 14*, which demonstrates the spectrum of frequencies generated by our custom power amplifiers. This illustration reveals that the power amplifier effectively eliminates various undesired distortion sounds that result from frequencies mixing together. The effectiveness of suppressing harmonics is proven by the reduction of the harmonic at 1.8 GHz, which decreased by 49 dB. However, at a frequency of 2.6 GHz, there was a reduction that could not be observed on the spectrum analyzer. This difference is attributed to each power amplifier's performance benefiting from an efficient control circuit designed for optimal second harmonic operation. The measured spectrum in *figure 16* closely resembles the spectrum presented in *figure 15(b).*

The displayed range of frequencies is generated by a power amplifier with two bands, which was constructed using a Keysight spectrum analyzer. In *table 2*, we can observe a comparison between the dual-band power amplifier and the single power amplifier in terms of phase rejection. Previous studies have demonstrated the effectiveness of the power amplifier in eliminating any signals it produces. These findings unequivocally demonstrate the soundness and reliability of the aforementioned approach.

In *table 3*, we can see the results of the amplifier and how it compares to others. What's interesting is that despite using a low-cost material called FR 4, this new approach shows effectiveness. The system operates with great efficacy in terms of accuracy and effectiveness, especially in relation to the elimination of signals.

Table 2. The proposal for the dual-band power amplifier was wrongly rejected.

False rejection	Single power amplifier	Dual-band power amplifier measured
Power out (f_2 - f_1) - Power out (f_1)	–4 dBc	–42 dBc
Power out (2 * f_1 – f_2) - Power out (f_1)	–16 dBc	–55 dBc
Power out (2 * f_1) - Power out (f_1)	–∞ dBc	-50 dBc
Power out (2 * f_2) - Power out (f_1)	–21 dBc	–∞ dBc
Power out (3 * f_1) - Power out (f_1)	–31 dBc	–47dBc

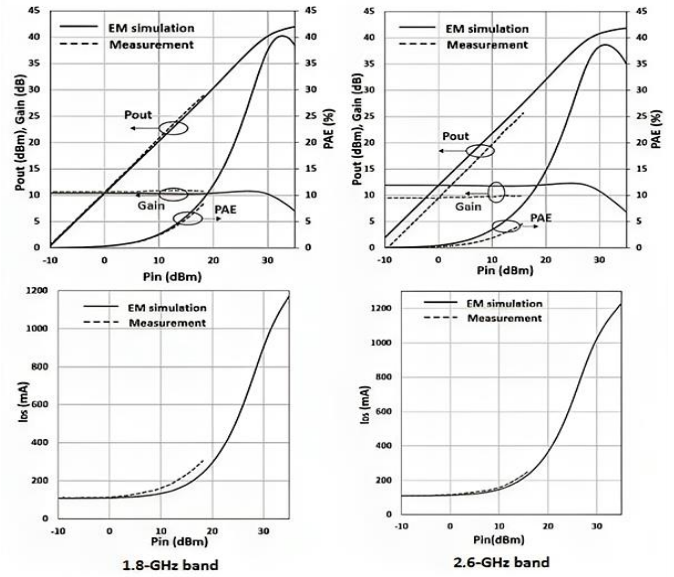

Figure 14: The exhibits provide data on both simulated and measured transfer characteristics, which show how the device responds to different input voltage levels. Additionally, they demonstrate the drain current characteristics, illustrating how the device's current fluctuates when different applied voltages are applied.

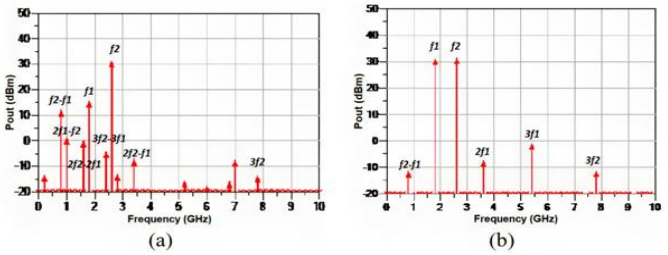

Figure 15: Results include: a) one power amplifier; b) a specially designed power amplifier that operates with two different frequency bands.

FOREX Publication
Open Access | Rapid and quality publishing
International Journal of Electrical and Electronics Research (IJEER)
Research Article | Volume 11, Issue 4 | Pages 979-987 | e-ISSN: 2347-470X

Table 3. Presents the differences between our proposed power amplifier and previous studies.

Ref.	[26]	[27]	[28]	[29]	This work
Frequency with f1 / f2	1.4/2.4	1.9/2.6	1.5/3.8	5.5/8.5	1.8/2.6
Power added efficiency with f1/ f2	65/65	72/66	47/52	71/74	40.2/38.7
Power out with f1 / f2	41/40	41.1/40.4	37.3/35.7	42/47	41.2/41.1
Gain with f1 /f2	13/12.5	10/10	15/10	21/19	10.2/10/1
Incorrect dismissal	N/A	N/A	N/A	–51with (3 * f1 – f2); –51 with 2 *f	– 59 with 2 * f1; – ∞ with 2 * f1; – 51 with (f2 – f1); – 64 with (2 * f1 – f2); – 56 with 3 *f1

4. RESULTS

The study yielded the following findings: The dual-band power amplifiers were able to achieve gains of 10.2 dB and 10.1 dB, output power (Pout) of 41.2 dBm and 41.1 dBm, and power-added efficiency (PAE) of 40.2% and 38.7% at frequencies of 1.8 GHz and 2.6 GHz, respectively. The second harmonic was suppressed by 49 dBc in the 1.8 GHz band, while in the 2.6 GHz band it was almost completely suppressed. The assessment of false rejections from the designed dual-band power amplifier confirms its ability to effectively eliminate unwanted mixing signal products in the output. The designed dual-band power amplifier exhibits exceptional linear performance by suppressing high-order and unwanted intermodulation distortion components. Experimental setups and measurements illustrate the properties of the power amplifiers that were designed, including power-added efficiency (PAE), output power, gain, and drain current (IDS). The performance of the dual-band amplifier that was designed is compared to that of other parallel-band amplifiers, which highlights its efficiency and linearity. The manifestation of this phenomenon can be attributed to the highly effective control circuits for the second harmonic in each power amplifier (PA). The graphical representation of the electromagnetic spectrum is presented in *figure 16*.

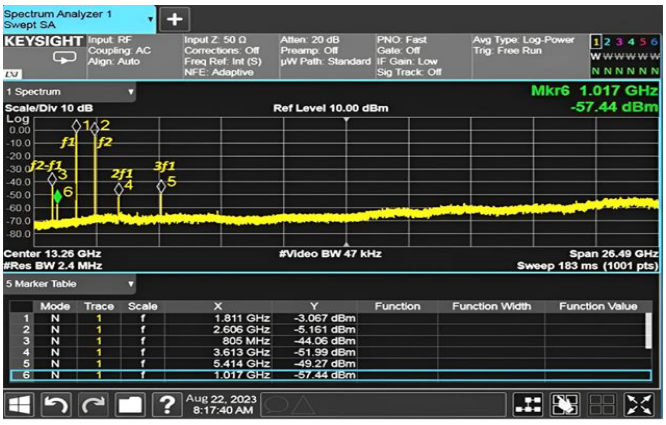

Figure 16: The comprehensive analysis of the high-frequency range produced by meticulously engineered dual-band amplifiers was thoroughly examined using the state-of-the-art spectrum analyzer offered by the renowned Keysight brand.

5. DISCUSSION

The discussion regarding the research paper centers around the creation of a cost-effective power amplifier that can function in two different frequency ranges for wireless communication systems. The amplifier operates at frequencies of 1.8 GHz and 2.6 GHz. The design incorporates techniques for signal separation and second harmonic suppression, resulting in a high level of efficiency and the ability to reject unwanted mixing products in both frequency bands. The developed amplifier demonstrates a gain of 10.2 dB and 10.1 dB, an output power of 41.2 dBm and 41.1 dBm, and a power enhancement efficiency of 40.2% and 38.7% at frequencies of 1.8 GHz and 2.6 GHz, respectively. Furthermore, the second harmonic reduction is measured at 49 dBc for 1.8 GHz and is almost entirely achieved for 2.6 GHz. The outcomes of the experiment confirm the amplifier's ability to eliminate undesired mixing signal products and suppress intermodulation distortion components, thus demonstrating its commendable linear performance. The performance of this dual-band power amplifier is subsequently compared to that of other dual-band amplifiers, thus illustrating its efficiency and linearity.

6. CONCLUSION

This scholarly article elucidates the process by which a power amplifier operating at two distinct frequencies, namely 1.8 GHz and 2.6 GHz, was designed. Segments of the signal, which encompass both frequencies, are systematically generated. These segments are then strengthened using a diplexer, which helps minimize signal loss and prevent interference. By utilizing suppression techniques, the power amplifier achieves efficiency. Maintains clean signals across multiple frequency ranges. The effectiveness of this amplifier has been evaluated using signals at a frequency of 1.8 GHz. It amplifies the signal by 10.2 decibels, resulting in an output power of 41.2 decibel milliwatts, while converting 40.2% of the input power into

International Journal of Electrical and Electronics Research (IJEER)
Research Article | Volume 11, Issue 4 | Pages 979-987 | e-ISSN: 2347-470X

output power. Similarly, at a frequency of 2.6 GHz, the amplification reaches a value of 10.1, resulting in an output power of 41.1 decibel milliwatts and an efficiency rating of 38.7%. For the 1.8 GHz band, there is a reduction in distortion of approximately 49 dB. In the case of the 2.6 GHz band, near complete elimination of harmonic distortion is observed. Furthermore, this proposed circuitry successfully addresses any combining or mixing issues that may arise at its endpoint. Overall, this power amplifier proves to be highly beneficial for communication systems, highlighting its importance.

Further optimization of the design of dual-band power amplifiers is necessary to enhance both efficiency and linear performance. The exploration of various circuit configurations and technologies is being undertaken to improve the suppression of unwanted mixing products and intermodulation distortion components. Additionally, alternative approaches are being considered for integrating end and signal split in order to achieve higher levels of second-order integration suppression and improved linearity. The performance evaluation of dual-band power amplifiers, specifically designed for real-world wireless communication systems, is being conducted to assess their performance in a realistic scenario. The possibility of implementing a dual-band power amplifier, designed using different substrates or technologies, is being investigated to assess its adaptability and potential for integration into various wireless communication systems. Further investigation is needed to examine the impact of various operational conditions and environmental factors on the performance of dual-band power amplifiers. This investigation is crucial for ensuring the reliability and robustness of amplifiers for practical applications.

Author Contributions: Wael Saad Ahmed is involved in tasks such, as brainstorming, researching, reviewing and editing. Nsaif Jasim Hadi Al Chaabawis responsibilities include conducting investigations developing methodologies and drafting content. Moreover, this individual has contributed to the research design and data analysis. Ahmed Atiyah Itwayya handles tasks related to brainstorming ideas organizing data writing (including reviewing and editing) securing funding and managing the project. It is important to highlight that all authors have thoroughly read and agreed to the version of the manuscript.

Acknowledgments: The task was accomplished with the support and collaboration of various individuals and organizations. We extend our sincere appreciation to all scholars who provided support and assisted us, and whose valuable advice and expertise throughout the entire research endeavor were acknowledged. Their observations and input significantly enhanced the quality of the task.

Conflicts of Interest: "The authors declare no conflict of interest."

Wael Saad Ahmed – lecturer at Tikrit University; assistant lecturer in the Medical Physics Branch at the College of Medicine, Tikrit University, Salahuddin, Iraq, e-mail: wael.alrawi@tu.edu.iq, ORCID: 0000-0003-1180-7857, Scopus Author ID: 58184429600.

Nsaif Jasim Hadi Al-Chaabawi – M.S.c. in Electronic Communication and Computer Engineering from Nottingham University, Nottingham, UK; Lecturer of Electrical Engineering Department, University of Misan; Head of the Systems and Software Division at the Computer Center, University of Misan; Lecturer of Petroleum Engineering Department, College of Engineering, Department of Petroleum, University of Misan, Amarah, Iraq, e-mail: nsf_jsm@uomisan.edu.iq, ORCID: 0000-0001-6776-2489, Scopus Author ID: 57234426900.

Ahmed Atiyah Itwayya – M.Sc. in Electronic Communication and Computer Engineering from Nottingham University, Nottingham, UK; I currently serve as the Head of the IT Department at the General Company for Southern Electricity Distribution, specifically at the Misan Branch. I am also a lecturer in the Electrical Engineering Department at the University of Misan. E-mail: eng.ahmed.rml@gmail.com, ORCID: 0000-0001-7573-9385, Scopus Author ID: 57214135735.

REFERENCES

[1] Fan, L., Hongxi, Y. & Xiaoxiao, L. Development overview of Sequential Power Amplifiers. IEEE International Workshop on Electromagnetics: Applications and Student Innovation Competition (iWEM), Guangzhou, China, 2021, pp. 1-3. DOI: 10.1109/iwem53379.2021.9790500.

[2] Hussein, S. & Yassin, M. Efficiency enhancement of CMOS power amplifier for RF applications. Al-Rafidain Engineering Journal (AREJ), 2022, vol. 27, iss. 2, pp. 60–67. DOI: 10.33899/rengj.2022. 132768.1156.

[3] Jin, Y., Zhijiang, D., Xiongbo, R., Changzhi, X. & Mingyu, L. A dual load-modulated Doherty power amplifier design method for improving power back-off efficiency. Sensors, 2023, vol. 23, iss. 14, article no. 6598. DOI: 10.3390/s23146598.

[4] Sear, W. & Barton, T. W. Power-amplifier stabilization through out-of-band feedback. IEEE Microwave and Wireless Components Letters, 2020, vol. 30, iss. 8, pp. 768–771. DOI: 10.1109/lmwc.2020.3002727.

[5] Nghiem, X. A. & Gajadharsing, J. Continuous Quasi-Load Insensitive Class-E Mode for Wideband Doherty Power Amplifiers. IEEE/MTT-S International Microwave Symposium – IMS 2023, San Diego, CA, USA, 2023, pp. 450-453. DOI: 10.1109/ims37964.2023.10188219.

[6] Saad, P. & Hou, R. Symmetrical load modulated balanced power amplifier with asymmetrical output coupling for load modulation continuum. IEEE Transactions on Microwave Theory and Techniques, 2022, vol. 70, iss. 4, pp. 2315-2327. DOI: 10.1109/tmtt.2022.3147843.

[7] Shi, J., Dai, W., Fang, X., Zhou, X., Sui, J., Xia, J. & Cheng, K.-K. M. Novel Wideband Fully Integrated GaN Power Amplifier Design Using a Hybrid Bandpass-Lowpass Output Matching Network. IEEE Microwave and Wireless Technology Letters, 2023, vol. 33, iss. 8, pp. 1187-1190. DOI: 10.1109/lmwt.2023.3281389.

[8] Varlamov, O. V. Theoretical Foundations for teaching the causes of non-linear distortions in modern high-efficiency transmitters. 2022 Intelligent Technologies and Electronic Devices in Vehicle and Road Transport Complex (TIRVED), Moscow, Russian Federation, 2022, pp. 1-10. DOI: 10.1109/tirved56496.2022.9965552.

[9] Wang, Z., Hu, S., Gu, L. & Lin, L. Review of Ka-Band Power Amplifier. Electronics, 2022, vol. 11, iss. 6, article no. 942. DOI: 10.3390/electronics11060942.

[10] Wen, H., Feng, W., Zhu, H., Che, W. & Xue, Q. Design of dual-band high efficiency and linearity Doherty power amplifier. 2022

International Journal of Electrical and Electronics Research (IJEER)
Research Article | Volume 11, Issue 4 | Pages 979-987 | e-ISSN: 2347-470X

International Conference on Microwave and Millimeter Wave Technology (ICMMT), Harbin, China, 2022, pp. 1-3. DOI: 10.1109/icmmt55580.2022.10022344.

[11] Zhou, X. Y., Chan, W. S., Chen, S. & Feng, W. J. Broadband highly efficient Doherty Power Amplifiers. IEEE Circuits and Systems Magazine, Fourthquarter, 2020, vol. 20, iss. 4, pp. 47–64. DOI: 10.1109/mcas.2020.3027221.

[12] Zhu, H., Zhang, Z., Gu, C. & Xuan, X. A high-relative-bandwidth Doherty power amplifier with modified load modulation network for wireless communications. Sensors, 2023, vol. 23, iss. 5, article no. 2767. DOI: 10.3390/s23052767.

[13] Tang, W., Li, X., Dai, J. Y., Jin, S., Zeng, Y., Cheng, Q. & Cui, T. J. Wireless Communications with programmable Metasurface: Transceiver Design and experimental results. China Communications, 2019, vol. 16, iss. 5, pp. 46–61. DOI: 10.23919/j.cc.2019.05.004.

[14] Zeng, Y., Wu, Q. & Zhang, R. Accessing from the sky: A tutorial on UAV Communications for 5G and beyond. Proceedings of the IEEE, 2019, vol. 107, iss. 12, pp. 2327-2375. DOI: 10.1109/jproc.2019.2952892.

[15] Agrawal, N., Darak, S. J. & Bader, F. Spectral coexistence of LDACS and DME: Analysis via hardware software co-design in presence of real channels and RF impairments. IEEE Transactions on Vehicular Technology, 2020, vol. 69, iss. 9, pp. 9837–9848. DOI: 10.1109/tvt.2020.3002978.

[16] Yan, R.-L., Zhang, J., Chen, R.-H., Guo, J.-N. & Yu, L.-Y. Transceiver design for two-user SIMO FSO communication systems over lognormal channels. International Conference on Optoelectronic and Microelectronic Technology and Application, Nanjing, China, 2020, vol. 11617, pp. 1-6. DOI: 10.1117/12.2585452.

[17] Herrera-Bustamante, J., Rodríguez-Ludeña, V., Correa-Mena, A. G. & Barragán-Guerrero, D. Design and implementation in USRP of a preamble-based synchronizer for OFDM Systems. 2020 IEEE ANDESCON, Quito, Ecuador, 2020, pp. 1-6. DOI: 10.1109/andescon50619.2020.9272183.

[18] Agrawal, N., Ambede, A., Darak, S. J., Vinod, A. P. & Madhukumar, A. S. Design and implementation of low complexity reconfigurable filtered-OFDM-based LDACS. IEEE Transactions on Circuits and Systems II: Express Briefs, 2021, vol. 68, iss. 7, pp. 2399-2403. DOI: 10.1109/tcsii.2021.3053367.

[19] Pavia, J. P., Velez, V., Ferreira, R., Souto, N., Ribeiro, M., Silva, J. & Dinis, R. Low Complexity Hybrid Precoding Designs for Multiuser mmWave/THz Ultra Massive MIMO systems. Sensors, 2021, vol. 21, iss. 18, article no. 6054. DOI: 10.3390/s21186054.

[20] Geng, Y. A novel waveform design for OFDM-based Joint Sensing and Communication System. IEEE 3rd International Symposium on Joint Communications & Sensing (JC&S), Seefeld, Austria, 2023, pp. 1-6. DOI: 10.1109/jcs57290.2023.10107516.

[21] Sharma D, Vishwakarma RK. A Miniaturized Dual-Band Modified Rectangular-Shaped Antenna for Wireless Applications 2022;10. https://doi.org/10.37391/ijeer.100421.

[22] Su, Y.-D., Athas, J., Lalam, N., Grainger, B. & Ohodnicki, P. Low-cost plasmonic fiber probe and wireless interrogation for Electric Power Equipment Temperature Sensing. Fiber Optic Sensors and Applications XVIII, 2022, vol. 12105, pp. 1-12. DOI: 10.1117/12.2617139.

[23] Sowe M, Konditi DBO, Langat PK. A Compact High-Gain Microstrip Patch Antenna with Improved Bandwidth for 5G Applications 2022;10. https://doi.org/10.37391/ijeer.100225.

[24] Yuan, C. & Zhou, L. Design of intelligent energy-saving lighting control system based on ZigBee and Nb-IoT technology. Second International Conference on Biomedical and Intelligent Systems (IC-BIS 2023), 2023, vol. 12724, pp. 1-7. DOI: 10.1117/12.2687761.

[25] Knowledge Management using IoT-Blockchain Technology: State of the Art 2022;10. https://doi.org/10.37391/ijeer.100223.

[26] Kalyan, R., Rawat, K. & Koul, S. K. Reconfigurable and concurrent dual-band Doherty power amplifier for Multiband and Multistandard Applications. IEEE Transactions on Microwave Theory and Techniques, 2017, vol. 65, iss. 1, pp. 198-208. DOI: 10.1109/tmtt.2016.2614930.

[27] Nguyen, D.-A., Bui, G. T. & Seo, C. Design of Highly-Efficient Dual-Band GaN HEMT Power Amplifier with Dual-Class E/F−1 Operation. 2023 IEEE/MTT-S International Microwave Symposium - IMS 2023, San Diego, CA, USA, 2023, pp. 215-218. DOI: 10.1109/ims37964.2023.10187949.

[28] Bui, G. T., Nguyen, D.-A. & Seo, C. A Novel Design of Dual-Band Inverse Class-F Shunt-Diode Rectifier for Energy Harvesting. IEEE Transactions on Circuits and Systems II: Express Briefs, 2023, vol. 70, iss. 7, pp. 2345-2349. DOI: 10.1109/tcsii.2023.3240501.

[29] Wei, M.-D., Hüssen, L. & Negra, R. Compact High-Efficient 2.4/5.8 GHz Concurrent Dualband Rectifier using Tapered Microstrip Lines. 2022 Wireless Power Week (WPW), Bordeaux, France, 2022, pp. 392-395. DOI: 10.1109/wpw54272.2022.9854004.